Chem. Res. Chin. Univ., 2015, 31(4), 590—596 doi: 10.1007/s40242-015-5006-5

Graphene/γ-AlOOH Hybrids as an Enhanced Sensing Platform for Ultrasensitive Stripping Voltammetric Detection of Pb(II)

FAN Wei, MIAO Yue'e and LIU Tianxi*

State Key Laboratory of Molecular Engineering of Polymers, Department of Macromolecular Science, Fudan University, Shanghai 200433, P. R. China

Abstract The reduced graphene oxide(RGO)/γ-AlOOH hybrids with different γ-AlOOH contents were successfully prepared *via* a facile one-pot hydrothermal method. In these hybrids, RGO acts as a conductive linker for improving electron transport, and γ-AlOOH nanoplatelets help to adsorb the target metal ions on the electrode surface, thus facilitating the electrochemical behavior of the hybrids. The sensitivity of as-prepared RGO/γ-AlOOH hybrids toward Pb(II) was tested by square wave anodic stripping voltammograms(SWASV) and the mass ratio of graphene to γ-AlOOH was optimized to improve the sensing performance of RGO/γ-AlOOH hybrids. Owing to the superior absorbability of γ-AlOOH for heavy metal ions and excellent electrical conductivity of graphene, the detection limit of the hybrids for heavy metal ions was found to be as low as 1.5×10^{-11} mol/L with optimized γ-AlOOH content in the hybrids. The experimental conditions, such as pH value, mass of electrode material, and deposition time were also investigated and optimized. The as-prepared RGO/γ-AlOOH hybrids demonstrate high electrochemical activity and good sensing performance, which offers an alternative platform for the electrochemical sensors.

Keywords Graphene; γ-AlOOH; Hybrid; Heavy metal ion; Electrochemical sensor

1 Introduction

Heavy metal ions, such as cadmium and lead, are regarded as a kind of the most harmful pollutants and even exposure to trace amounts of heavy metal ions can result in toxicity[1]. Therefore, exploring the efficient, rapid and simple analytical methods for the precise monitoring of heavy metal ions is urgently needed. Various analytical techniques including solid phase spectrophotometry(SPS)[2], flame atomic absorption spectrometry(FASS)[3], atomic absorption spectrometry(AAS)[4], surface enhanced Raman spectrometry(SERS)[5], inductively coupled plasma atomic emission spectrometry or mass spectrometry(ICP-AES or ICP-MS)[6] are available for the detection of heavy metal ions. However, these spectrometric methods often require sophisticated operation and expensive instruments, which limits their application to laboratory level only. In contrast, the electrochemical method has attracted a growing interest of some scientists because of its high sensitivity, portability, accurateness, fast analysis speed, favorable stability and low cost[7—9]. Among all the electrochemical methods, anodic stripping voltammetry(ASV) has been widely recognized as an effective technique for the quantification of trace metal ions due to an effective preconcentration step followed by electrochemical stripping measurement of the accumulated analytes[10,11]. As is known, its sensing performance is closely related to the amount of metal ions preconcentrated on the surface of the electrode, which mainly depends on the electroactivity and adsorption capacity of the sensing material[12,13]. Hence, it is of great interest and importance to develop efficient electrochemical sensors based on novel materials with excellent sensing performance.

Graphene, a monolayer of sp^2 hybridized carbon atoms, has attracted great attention due to its fascinating physical and electrochemical properties[14—16]. Especially, it has been widely applied in electrochemical sensing fields as a promising electrode material, in terms of large surface area, extraordinary electrical properties and high electrocatalytic activities[17—19]. It can exhibit a comparable wide electrochemical potential window and a lower charge-transfer resistance than glassy carbon and graphite electrodes[20—22]. Consequently, an electrochemical sensor based on Nafion-graphene film has been developed, which shows a detection limit of 0.1 nmol/L for Pb^{2+} in aqueous solution[23]. However, the graphene nanosheets, usually obtained from the reduction of graphene oxide(GO)[24—27], have a strong tendency to form irreversible aggregation due to van der Waals interactions and strong π-π stacking, which significantly limits its intrinsic distinguished properties and inhibits their application in electrochemical analysis[28,29]. One effective method to solve this problem is to incorporate nanomaterials into graphene sheets, which can minimize or prevent the aggregation of graphene sheets. Consequently, graphene-based nanocomposites have been studied for electrochemical sensing, which show significant improvement in properties compared with conventional composites or pure graphene[30—34]. For example, Wei *et al*.[35] fabricated SnO_2/reduced graphene oxide(RGO) nanocomposite for electrochemical detection of

*Corresponding author. E-mail: txliu@fudan.edu.cn

Received January 5, 2015; accepted May 19, 2015.

Supported by the National Natural Science Foundation of China(No.51125011).

Pb(II), Cd(II), Hg(II) and Cu(II) in drinking water, with detection limits of 1.8×10^{-10}, 1.0×10^{-10}, 2.8×10^{-10} and 2.3×10^{-10} mol/L, respectively. Sun *et al.*[36] used Fe_3O_4-RGO modified electrode for Cd^{2+} detection, which showed a detection limit of 0.056 μmol/L. Lei *et al.*[37] realized the determination of hydrazine with MnO_2/GO composite, which showed a sensitivity of 1.0 $mA\cdot L\cdot mmol^{-1}\cdot cm^{-2}$ and a detection limit of 0.16 μmol/L.

As reported previously, it was found that γ-AlOOH (boehmite) has a high adsorption capacity toward heavy metal ions, such as Pb(II) and Cd(II)[38]. However, its electrochemical activity is greatly inhibited by its low electrical conductivity. To solve this problem, Gao *et al.*[39] synthesized the γ-AlOOH-RGO nanocomposites which combined the advantages of excellent electrical conductivity of graphene and the superior absorbability of γ-AlOOH. The nanocomposites show a detection limit of 9.3×10^{-11} mol/L for Pb(II) and 3.5×10^{-11} mol/L for Cd(II), respectively. Herein, we tried to further improve the sensing performance of RGO/γ-AlOOH hybrids by optimizing the mass ratio of graphene to γ-AlOOH. The RGO/γ-AlOOH hybrids with different γ-AlOOH contents[*i.e.*, 30%(mass fraction), 51% and 72% in our case] have been successfully synthesized *via* a facile one-pot hydrothermal method. Through the hydrothermal reaction, γ-AlOOH nanoplatelets are homogeneously precipitated on GO surface and GO can be reduced to graphene(*i.e.*, RGO) simultaneously. TEM images of RGO/γ-AlOOH hybrids show the morphology diversity as the γ-AlOOH content changes. And the RGO/γ-AlOOH hybrid with 51% γ-AlOOH nanoplatelets shows a superior sensitivity toward Pb(II) with a detection limit as low as 1.5×10^{-11} mol/L. Therefore, the RGO/γ-AlOOH hybrids thus prepared with excellent sensitivity, reproducibility and stability, offer an alternative platform for heavy metal ions detection in terms of electrochemical sensing.

2 Experimental

2.1 Materials

Natural graphite powder(325 meshes) was supplied by Alfa-Aesar. Aluminium(III) chloride ($AlCl_3$), uera, and ethanol were purchased from China Medicine Co. All the chemicals were used as received without further treatment. Deionized water was used throughout all the experiments.

2.2 Synthesis of GO

GO was synthesized from natural graphite powder *via* a modified Hummers method[40]. The resulting GO solid was dispersed in water by ultrasonication under ambient conditions for 30 min to make a homogeneous GO aqueous dispersion.

2.3 Fabrication of RGO/γ-AlOOH Hybrids

RGO/γ-AlOOH hybrids were synthesized with a hydrothermal method. Typically, different amounts of $AlCl_3$ and urea were added to 0.5 mg/mL GO aqueous suspension. Subsequently, the mixed suspension was ultrasonicated for 30 min followed by transferring into a 100 mL Teflon-lined stainless steel autoclave and maintained at 180 °C for 3 h. After the autoclave was cooled down to room temperature, the resulting product was isolated by centrifugation, washed several times with water and ethanol, respectively, followed by drying at 60 °C under vacuum. The as-prepared RGO/γ-AlOOH hybrids with different γ-AlOOH contents(30%, 51% and 72%) were denoted as GA-1, GA-2 and GA-3, respectively. All the preparation processes are illustrated in Scheme 1. For comparison, γ-AlOOH or RGO was prepared by the same procedure without adding GO dispersion or $AlCl_3$ and urea.

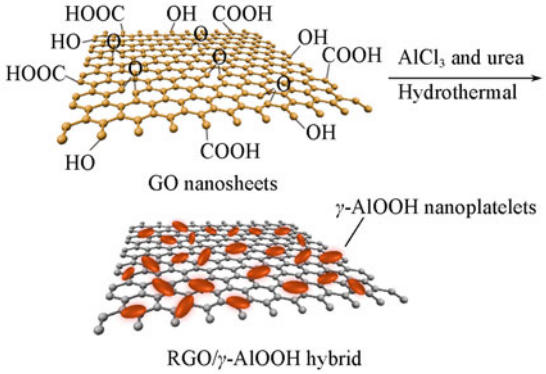

Scheme 1 Schematic illustration of preparation process for RGO/γ-AlOOH hybrids

2.4 Characterization

X-Ray diffraction(XRD) patterns were obtained on an X'Pert Pro X-ray diffractometer with Cu *Kα* radiation (λ=0.1542 nm) at a voltage of 40 kV and a current of 40 mA. Morphology of the sample was investigated under transmission electron microscope(TEM, JEOL 2100) at an accelerating voltage of 200 kV. Thermogravimetric analysis(TGA, Pyris 1) was carried out under air flow from 100 °C to 800 °C at a heating rate of 10 °C/min. X-Ray photoelectron spectroscopy (XPS) measurement was carried out on an RBD upgraded PHI-5000C ESCA system(Perkin Elmer) with a monochromatic Al *Kα* radiation(*hv*=1486.6 eV). All the XPS spectra were corrected with the C_{1s} line at 284.6 eV.

2.5 Electrochemical Measurement

The hybrid sample was dripped onto a glassy carbon electrode(GCE, ϕ=3 mm) surface that served as the working electrode. Typically, 5 μL of 1.0 mg/mL dispersion of RGO/γ-AlOOH hybrid was casted onto the GCE surface, followed by drying naturally at room temperature to get the hybrid sample modified GCE.

Electrochemical tests were carried out on a CHI 660C electrochemical workstation(Chenhua Instruments Co., Shanghai, China). A three-electrode system was used, consisted of the sample modified GCE as the working electrode, Ag/AgCl electrode as the reference electrode, and platinum as the counter electrode. Square wave anodic stripping voltammetry(SWASV) was used for the detection of Pb(II) with optimized parameters. Pb was accumulated at a potential of –1.1 V for 120 s by the reduction of Pb(II) in 0.1 mol/L NaAc-HAc. The anodic stripping of electrodeposited Pb was performed in a potential range of –1.3 V to 0.5 V at a frequency of 15 Hz and an amplitude of

25 mV.

3 Results and Discussion

3.1 Morphological and Structural Characterization of RGO/γ-AlOOH Hybrids

RGO/γ-AlOOH hybrids were synthesized directly from GO and $AlCl_3$ in the presence of urea by the hydrothermal method, as schematically illustrated in Scheme 1. Firstly, Al^{3+} ions were absorbed on the surface of GO nanosheets through electrostatic interaction between positively charged Al^{3+} ions and negatively charged oxygen-containing functional groups (—OH or —COOH) on GO. Under heating conditions, urea could release CO_2 and OH^-, which would react with Al^{3+} ions to form $Al(OH)_3$ on the surface of GO nanosheets. The relevant reactions for the formation of γ-AlOOH are listed as follows:

$$CO(NH_2)_2+3H_2O \longrightarrow 2NH_4^+ + CO_2 + 2OH^- \quad (1)$$

$$Al^{3+}+3OH^- \longrightarrow Al(OH)_3 \quad (2)$$

$$Al(OH)_3 \longrightarrow AlOOH+H_2O \quad (3)$$

At the same time, pristine GO nanosheets were simultaneously reduced to RGO after the hydrothermal reaction. Under hydrothermal conditions, supercritical water can play the role of reducing agent and allow the catalysis of a variety of heterolytic(ionic) bond cleavage reactions in water. Therefore, both intramolecular as well as intermolecular dehydration can occur on the edges or basal planes of GO in the presence of supercritical water under hydrothermal conditions[41,42]. In addition, the γ-AlOOH inserted in the graphene nanosheets could prevent RGO from restacking during reduction effectively. Thus, the as-prepared RGO/γ-AlOOH hybrids with a high active surface area can contribute to better electrochemical performance, which will be proved in later sections.

Fig.1 displays the representative XRD patterns of the as-obtained samples. GO displays a typical diffraction peak at 2θ=10.6° corresponding to an much larger interlayer distance of 0.81 nm than graphite does(0.34 nm) owing to the abundant oxygenated functional groups introduced on graphene sheets. In contrast, the peak at 2θ=10.6° disappears and a broad peak at 2θ=24.8° appears for RGO, indicating that GO was successfully reduced after hydrothermal treatment. The XRD pattern of γ-AlOOH containing 4 sharp peaks, which represent the (020), (120), (031) and (200) crystal planes, is consistent with the standard XRD patterns of orthorhombic AlOOH(JCPDS No. 01-074-1895). GA-2 hybrid shows a diffraction pattern similar to that of γ-AlOOH with an additional characteristic (002) peak of graphene, indicating the coexistence of γ-AlOOH and graphene in the hybrid. In addition, the reduction of GO is also confirmed by Raman spectra. As shown in Fig.2, GO displays two prominent peaks at 1340 and 1597 cm^{-1}, corresponding to the well-documented D and G bands, respectively[43]. Although the Raman spectrum of RGO also exhibits both D and G bands, the intensity ratio of D/G increases from 1.21 for GO to 1.34 for RGO, implying a decreased size of the sp^2 domains for GO upon hydrothermal reduction[44].

Fig.3(A) illustrates the typical TEM image of GO, revealing a few micrometers in size and slightly crumpled and

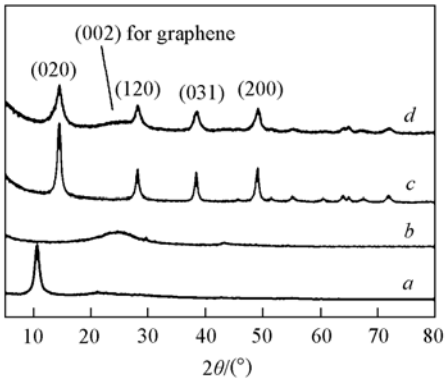

Fig.1 XRD patterns of GO(*a*), RGO(*b*), γ-AlOOH(*c*) and GA-2 hybrid(*d*)

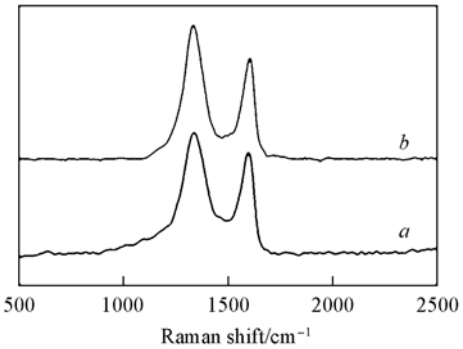

Fig.2 Raman spectra of GO(*a*) and RGO(*b*)

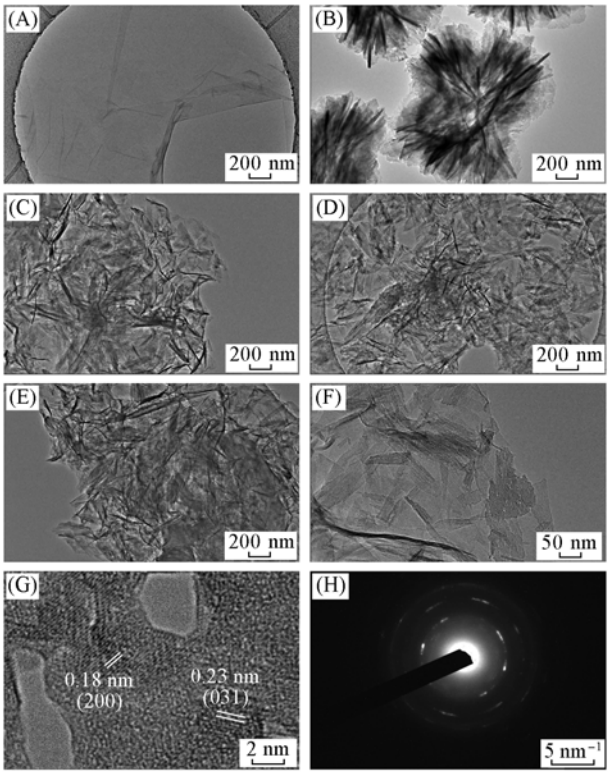

Fig.3 TEM images of GO(A), γ-AlOOH(B), GA-1 hybrid(C), GA-2 hybrid(D), GA-3 hybrid(E), and the corresponding image at high magnification(F), high-resolution TEM image(G) and SAED pattern(H) of GA-2 hybrid

rippled on sheet edges. Fig.3(B) presents neat γ-AlOOH nanoplatelets with a length of about 400—500 nm and these nanoplatelets tend to be closely packed into flower-like architectures. In contrast, for RGO/γ-AlOOH hybrids as shown in Fig.3(C)—(F), γ-AlOOH nanoplatelets are evenly immobilized on both the sides of the two-dimensional RGO sheets. Graphene can afford an effective substrate to prevent γ-AlOOH from agglomeration and enable a uniform dispersion and distribution of γ-AlOOH nanoplatelets over its support. Different from pure γ-AlOOH nanoplatelets, the γ-AlOOH nanoplatelets grown on RGO nanosheets exhibit much thinner and loose lamellar structures, as shown in the high magnification TEM image[Fig.3(F)]. Conversely, γ-AlOOH nanoplatelets inserted between graphene layers also greatly prevent RGO nanosheets from restacking, ensuring the effective utilization of active surface area. Furthermore, most of RGO nanosheets are decorated with γ-AlOOH nanoplatelets, and even no individual γ-AlOOH nanoplatelets are observed outside the graphene sheets. For GA-1 sample[Fig.3(C)], there is still some blank area on RGO nanosheets. With the increase of mass fraction of γ-AlOOH, much more γ-AlOOH nanoplatelets can be observed. And almost a monolayer of γ-AlOOH nanoplatelets covers uniformly on RGO nanosheets[Fig.3(D)]. Further increasing the γ-AlOOH content leads to some aggregates formed on the RGO nanosheets, as shown in Fig.3(E), which will reduce the effective surface area. Besides, the high-resolution TEM image[Fig.3(G)] and selected area electron diffraction(SAED) pattern[Fig.3(H)] of GA-2 hybrid show the high crystallinity of γ-AlOOH. As indexed in Fig.3(G), the interatomic distances were determined to be 0.18 and 0.23 nm, respectively, corresponding to the (200) and (031) planes, and they match well with the XRD results.

Fig.4 exihibits the XPS spectra of GO, γ-AlOOH and GA-2 hybrid. It can be seen that compared with that of GO, there are two extra peaks located at 118.7 and 74.1 eV in the XPS spectrum of GA-2 hybrid, which correspond to Al_{2s} and Al_{2p}[45]. Such peaks could confirm that γ-AlOOH does exist in the hybrid. Fig.4(B) displays the high-resolution Al_{2p} spectrum of the hybrid. The C_{1s} spectra of GO[Fig.4(C)] present five different peaks observed at 284.5, 285.6, 286.7, 287.8, and 288.8 eV, which can be attributed to sp^2C, sp^3C, —C—O, —C═O, and COO^- groups, respectively. Compared with those of GO, the intensities of the C_{1s} peaks of the —C—O, —C═O and COO^- groups of GA-2 hybrid decrease dramatically, indicating the successful removal of the oxygen-containing functional groups and the well-restored conjugated graphene sheets after the hydrothermal process. The removal of oxygen-containing functional groups could ensure the good electrical conductivity of RGO sheets, which can form conductive networks between adjacent γ-AlOOH nanoplatelets.

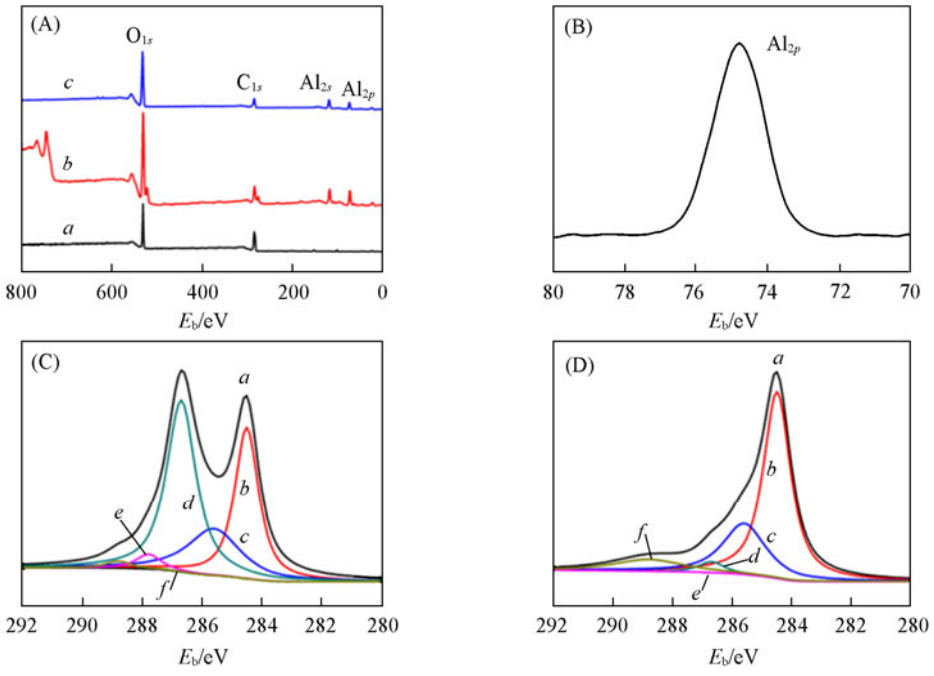

Fig.4 XPS spectra of GO(*a*), γ-AlOOH(*b*) and GA-2 hybrid(*c*)(A), high-resolution Al_{2p} spectrum of GA-2 hybrid(B) and C_{1s} spectra of GO(C) and GA-2 hybrid(D), respectively

(C) and (D) *a*. Sum; *b*. sp^2C; *c*. sp^3C; *d*. —C—O; *e*. —C═O; *f*. COO^-.

The compositions of GA-1, GA-2 and GA-3 hybrids were further investigated by TGA. As shown in Fig.5, GO displays a two-step mass loss in air. The first stage is from 200 °C to 300 °C, attributing to the removal oxygen-containing functional groups on the surface. The second stage is assigned to the complete decomposition of carbon skeleton, starting at about 550 °C[46]. In contrast, RGO shows only a one-step mass loss and the decomposition temperature is 70 °C higher than that of GO, indicating an improved thermal stability. This further proves the successful reduction of GO during the hydrothermal process. γ-AlOOH shows a slight mass loss when heated to 800 °C, which can be attributed to its decomposition into Al_2O_3 and water[47]. From the TGA results, the γ-AlOOH contents of GA-1, GA-2 and GA-3 hybrids are estimated to be 30%, 51% and 72%, respectively.

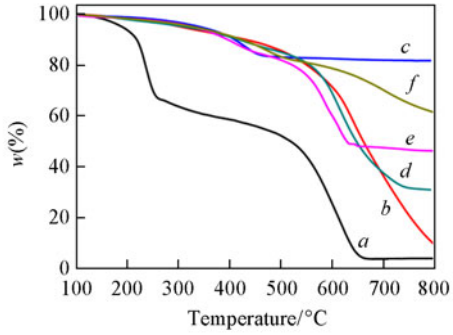

Fig.5 TGA curves of GO(*a*), RGO(*b*), γ-AlOOH(*c*), and GA-1(*d*), GA-2(*e*) and GA-3(*f*) hybrids

3.2 Experimental Condition Optimization of RGO/γ-AlOOH Hybrids Based Electrode for Pb(II) Detection

RGO/γ-AlOOH hybrids prepared above combine the advantages of graphene with those of γ-AlOOH, resulting in improved electrical conductivity and high adsorption capacity of them for metal ions. These merits thus offer the opportunity to utilize the hybrid material for electrochemical sensing with high sensitivity and stability. The sensing behavior of the as-prepared RGO/γ-AlOOH hybrid-based electrode toward trace metal ions, such as Pb(II), in aqueous solution, was studied in detail as follows by the technique of SWASV.

In order to get the maximum sensing performance, the experimental conditions, such as the mass of the electrode material, deposition time and pH value were then optimized. Fig.6(A) shows the effect of the mass of loaded GA-2 hybrid on SWASV response in the presence of 0.5 μmol/L Pb(II) in 0.1 mol/L NaAc-HAc(pH=5.0). Well-defined peak at a potential of −0.52 V was observed and the highest stripping current was found as 5 μg of hybrid was used. The stripping current decreased with further increasing the mass of GA-2 hybrid on the electrode. This may tentatively be attributed to worse film stability and a reduced electrical connectivity within the thicker film. Decreasing the mass of GA-2 hybrid beyond 5 μg results in a lower adsorption amount of Pb(II) and a dramatical reduction of the sensitivity in response to Pb(II). Therefore, unless otherwise stated, 5 μg of hybrid material was used throughout.

Fig.6(B) depicts the effect of the deposition time for Pb(II)

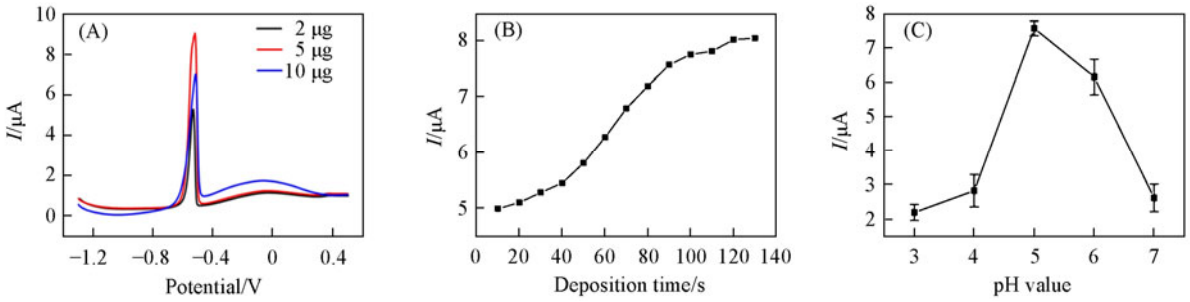

Fig.6 Effects of mass of loaded GA-2 hybrid(A), deposition time for Pb(II)(B) and pH(C) on SWASV response in the presence of 0.5 μmol/L Pb(II) in 0.1 mol/L NaAc-HAc

on voltammetric response. As shown above, stripping peak current increases with the extending of the deposition time varying from 10 s to 130 s. However, increasing deposition time will cause the decrease of the upper detection limit due to the surface saturation. As a result, to pursue a balance between the sensitivity and the detection limit, an optimal deposition time of 120 s was chosen in our condition.

In the stripping analysis, pH value also has an effect on the stripping current and thus affects the detection limit and sensitivity. Fig.6(C) depicts the relationship between pH value and stripping peak current. As shown in Fig.6(C), when the pH value increases from 3.0 to 5.0, the peak current increases, and then decreases as the pH value further increases from 5.0 to 7.0. It was previously reported that the adsorption capacity of γ-AlOOH almost reached maximum as the pH value was about 4.0—5.0[38]. Thus, at this pH value, the GA-2 hybrid can much easier capture Pb(II) and subsequently collect it on the electrode surface. Therefore, pH=5.0 in NaAc/HAc buffer solution was chosen as the optimal pH for the stripping tests.

3.3 Stripping Behaviour Toward Pb(II) of RGO/γ-AlOOH Hybrids

Fig.7 displays the SWASV response of bare GCE, RGO, γ-AlOOH, and GA-1, GA-2 and GA-3 hybrids modified GCE in a solution containing 0.5 μmol/L Pb(II). As observed from Fig.7, there was almost no response for bare GCE(curve *a*) in a voltage range from −1.3 V to +0.5 V. As for RGO(curve *b*) and γ-AlOOH nanoplatelets(curve *c*) modified GCE, there was only one weak peak of Pb(II) located at a potential of −0.52 V, which could be attributed to the high conductivity but inferior absorbability of RGO and the low conductivity but superior absorbability of γ-AlOOH. Nevertheless, all the three RGO/γ-AlOOH hybrids show a much sharper and higher peak of Pb(II) compared to the individual components. This is mainly due to the synergistic effect of the high conductivity of

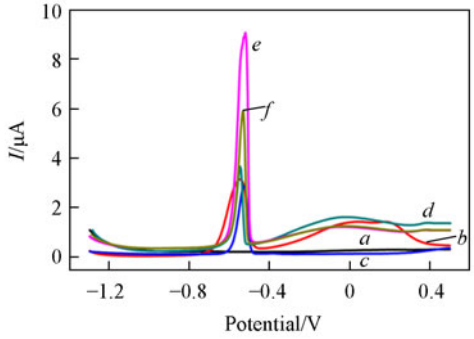

Fig.7 SWASV response of bare GCE(*a*), RGO(*b*), γ-AlOOH(*c*), and GA-1(*d*), GA-2(*e*) and GA-3(*f*) hybrids modified GCE

graphene and superior absorbability of γ-AlOOH. It should be noted that GA-2 hybrid shows the most significant response to Pb(II) among the three hybrid samples, which can be attributed to an optimized amount of γ-AlOOH homogeneously dispersed on the RGO sheets. With less γ-AlOOH content, the GA-1 hybrid exhibits weaker adsorption ability toward the target heavy metal ions. However, further increasing the γ-AlOOH content results in aggregates[Fig.3(E)], which will hinder the effective surface area. Therefore, the GA-2 hybrid was selected for further electrochemical experiments.

Fig.8(A) shows the SWASV response and the corresponding calibration curve of GA-2 hybrid/GCE electrode toward Pb(II) at different concentrations[inset in Fig.8(A)]. The well-defined peak of Pb(II) was observed at a potential of approximately –0.52 V. And the stripping peak current increases with the concentration increase of Pb(II) obviously from 0.01 μmol/L to 1 μmol/L. The calibration curve displays a linear relationship with a correlation coefficient of 0.998. The calculated limit of detection(LOD) is about 1.5×10^{-11} mol/L(3σ method), which is greatly lower in comparison with those of other carbonaceous materials in terms of heavy metal ions detection[39]. The obtained LODs are much lower than that of the guideline(10 μg/L, 4.8×10^{-8} mol/L) given by the World Health Organization(WHO). The reproducibility of the proposed sensor was also investigated, as shown in Fig.8(B). The relative standard deviation(RSD) in response to the electrochemical sensing of Pb(II) is approximately 2.4%, showing a reasonable reproducible signal. Therefore, the RGO/γ-AlOOH hybrid modified electrode manifests an excellent stability and reproducibility for repetitive electrochemical detection of metal ions.

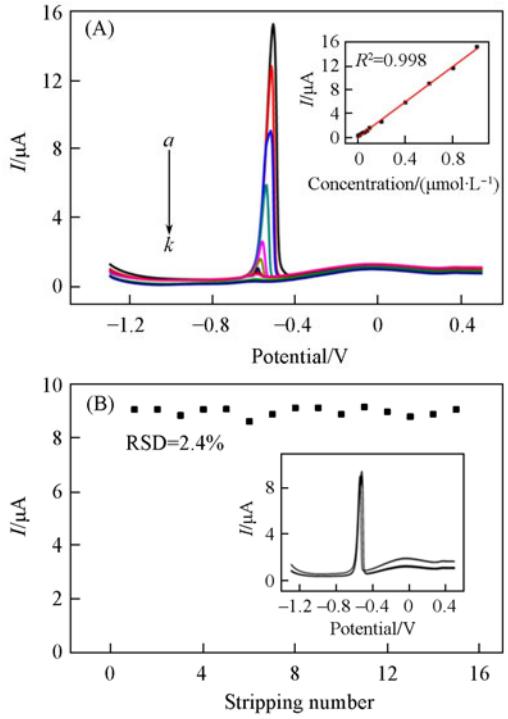

Fig.8 SWASV response of GA-2 electrode toward Pb(II) at different concentrations in 0.1 mol/L NaAc-HAc(pH=5.0)(A) and the stability of repetitive measurements 15 times of SWASV response toward 0.5 μmol/L Pb(II) on the GA-2 hybrid modified GCE(B)

c[Pb(II)]/(μmol·L^{-1}): *a*. 1; *b*. 0.8; *c*. 0.6; *d*. 0.4; *e*. 0.2; *f*. 0.1; *g*. 0.08; *h*. 0.06; *i*. 0.04; *j*. 0.02; *k*. 0.01. The inset of (A) is plot of current *versus* Pb(II) concentration. The inset of (B) is the SWASV response of 15 different stripping times.

4 Conclusions

In this study, the RGO/γ-AlOOH hybrids were successfully synthesized *via* a green and facile hydrothermal method. By combining the excellent electrical conductivity of graphene with the high adsorption capacity of γ-AlOOH, the RGO/γ-AlOOH hybrids become promising electrode materials for heavy metal ions detection. Furthermore, the sensing performance of the hybrids is optimized by controlling the amount of γ-AlOOH nanoplatelets on RGO nanosheets. The RGO/γ-AlOOH hybrid with 51% γ-AlOOH nanoplatelets shows superior sensitivity toward Pb(II) with a detection limit as low as 1.5×10^{-11} mol/L. These results demonstrate that the loaded amount has great influences on the sensing performance of the hybrids, indicating that proper nano-engineering of the hybrid structure is the key to realize its full performance. Therefore, this work highlights the great potential of using RGO/γ-AlOOH hybrids with excellent sensitivity, reproducibility and stability as an alternative platform for electrochemical sensing in terms of heavy metal ions detection.

References

[1] Aragay G., Merkoçi A., *Electrochim. Acta*, **2012**, *84*, 49
[2] Amin A. S., Gouda A. A., *Food Chem.*, **2012**, *132*, 518
[3] Soylak M., Aydin A., *Food Chem. Toxicol.*, **2011**, *49*, 1242
[4] Bagheri H., Afkhami A., Saber-Tehrani M., Khoshsafar H., *Talanta*, **2012**, *97*, 87
[5] Ma Y., Liu H., Qian K., Yang L., Liu J., *J. Colloid Interf. Sci.*, **2012**, *386*, 451
[6] Zhao L., Zhong S., Fang K., Qian Z., Chen J., *J. Hazard. Mater.*, **2012**, *239*/*240*, 206
[7] Arpadjan S., Çelik G., Taşkesen S., Güçer Ş., *Food Chem. Toxicol.*, **2008**, *46*, 2871
[8] Gómez Y., Fernández L., Borrás C., Mostany J., Scharifker B., *Talanta*, **2011**, *85*, 1357
[9] Li M., Li D., Li Y., Xu D., Long Y., *Anal. Chim. Acta*, **2011**, *701*, 157
[10] Jain A. K., Gupta V. K., Singh L. P., Raisoni J. R., *Electrochim. Acta*, **2006**, *51*, 2547
[11] Lin Z., Li X., Kraatz H., *Anal. Chem.*, **2011**, *83*, 6896
[12] Alves G. M. S., Magalhães J. M. C. S., Salaün P., van den Berg C. M. G., Soares H. M. V. M., *Anal. Chim. Acta*, **2011**, *703*, 1
[13] Richardson J., Drake A., Lazo-Miller C., Hand J., Morgan T., Lagadic I., *Sensors Actuat. B: Chem.*, **2011**, *158*, 271
[14] Novoselov K. S., *Science*, **2004**, *306*, 666
[15] Ma C., Chen Z., Fang M., Lu H., *J. Nanopart. Res.*, **2012**, *14*, 996
[16] Xu H. H., Wang X. L., Chen R., Yu Z. Y., *Chem. Res. Chinese Universities*, **2012**, *30*(2), 205
[17] Wang Z., Liu E., *Talanta*, **2013**, *103*, 47
[18] Chang H., Wu H., *Energy Environ. Sci.*, **2013**, *6*, 3483
[19] Wu S., He Q., Tan C., Wang Y., Zhang H., *Small*, **2013**, *9*, 1160

[20] Jian J., Liu Y., Zhang Y., Guo X., Cai Q., *Sensors*, **2013**, *13*, 13063
[21] Zhang J., Jin Z., Li W., Dong W., Lu A., *J. Mater. Chem. A*, **2013**, *1*, 13139
[22] Chao H., Fu L., Li Y., Li X., Du H., Ye J., *Electroanal.*, **2013**, *25*, 2238
[23] Li J., Guo S., Zhai Y., Wang E., *Anal. Chim. Acta*, **2009**, *649*, 196
[24] Wang B., Luo B., Liang M., Wang A., Wang J., Fang Y., Chang Y., Zhi L., *Nanoscale*, **2011**, *3*, 5059
[25] Wang B., Chang Y., Zhi L., *New Carbon Mater.*, **2011**, *26*, 31
[26] Gupta V. K., Yola M. L., Atar N., Ustundağ Z., Solak A. O., *Electrochim. Acta*, **2013**, *112*, 541
[27] An J. H., Park S. J., Kwon O. S., Bae J., Jang J., *ACS Nano*, **2013**, *7*, 10563
[28] Williams G., Seger B., Kamat P. V., *ACS Nano*, **2008**, *2*, 1487
[29] Liu J., Fu S., Yuan B., Li Y., Deng Z., *J. Am. Chem. Soc.*, **2010**, *132*, 7279
[30] Willemse C. M., Tlhomelang K., Jahed N., Baker P. G., Iwuoha E. I., *Sensors*, **2011**, *11*, 3970
[31] Zhang Y., Sun X., Zhu L., Shen H., Jia N., *Electrochim. Acta*, **2011**, *56*, 1239
[32] Wen Y., Peng C., Li D., Zhuo L., He S., Wang L., Huang Q., Xu Q., Fan C., *Chem. Commun.*, **2011**, *47*, 6278
[33] Gong J., Zhou T., Song D., Zhang L., *Sensors Actuat. B: Chem.*, **2010**, *150*, 491
[34] Zhu L., Xu L., Huang B., Jia N., Tan L., Yao S., *Electrochim. Acta*, **2014**, *115*, 471
[35] Wei Y., Gao C., Meng F. L., Li H. H., Wang L., Liu J. H., Huang X. J., *J. Phys. Chem. C*, **2012**, *116*, 1034
[36] Sun Y., Chen W., Li W., Jiang T., Liu J., Liu Z., *J. Electroanal. Chem.*, **2014**, *714*/*715*, 97
[37] Lei J., Lu X., Wang W., Bian X., Xue Y., Wang C., Li L., *RSC Advances*, **2012**, *2*, 2541
[38] Wei Y., Yang R., Zhang Y., Wang L., Liu J., Huang X., *Chem. Commun.*, **2011**, *47*, 11062
[39] Gao C., Yu X., Xu R., Liu J., Huang X., *ACS Appl. Mater. Interfaces*, **2012**, *4*, 4672
[40] Kovtyukhova N. I., Ollivier P. J., Martin B. R., Mallouk T. E., Chizhik S. A., Buzaneva E. V., Gorchinskiy A. D., *Chem. Mater.*, **1999**, *11*, 771
[41] Zhou Y., Bao Q., Tang L. A. L., Zhong Y., Loh K. P., *Chem. Mater.*, **2009**, *21*, 2950
[42] Xu Y. X., Sheng K. X., Li C., Shi G. Q., *ACS Nano*, **2010**, *4*, 4324
[43] Guo H., Wang X., Qian Q., Wang F., Xia X., *ACS Nano*, **2009**, *3*, 2653
[44] Stankovich S., Dikin D. A., Piner R. D., Kohlhaas K. A., Kleinhammes A., Jia Y., Wu Y., Nguyen S. T., Ruoff R. S., *Carbon*, **2007**, *45*, 1558
[45] Suchanek W. L., Garcés J. M., Fulvio P. F., Jaroniec M., *Chem. Mater.*, **2010**, *22*, 6564
[46] Lin Z., Yao Y., Li Z., Liu Y., Li Z., Wong C., *J. Phys. Chem. C*, **2010**, *114*, 14819
[47] Kuang D., Fang Y., Liu H., Frommen C., Fenske D., *J. Mater. Chem.*, **2003**, *13*, 660